Wheel-structured Triboelectric Nanogenerators with Hyperelastic Networking for High-Performance Wave Energy Harvesting

Yuchen Hu, Huijing Qiu, Qijun Sun, Zhong Lin Wang,* and Liang Xu*

Developing clean and renewable energy sources is an important strategy to reduce carbon emission and achieve carbon neutrality. As one of the most promising clean energy sources, large-scale, and efficient utilization of ocean blue energy remains a challenging problem to be solved. In this work, a hyperelastic network of wheel-structured triboelectric nanogenerators (WS-TENGs) is demonstrated to efficiently harvest low-frequency and small-amplitude wave energy. Different from traditional designs of smooth shell, the external blades on the TENG allow tighter interaction between the wave and the device, which can roll on the water surface like a wheel, continuously agitating internal TENGs. Moreover, the hyperelastic networking structure can stretch and shrink like a spring with stored wave energy, further intensifying the roll of the device, and connecting the WS-TENGs to form a large-scale network. Multiple driving modes with synergistic effects can be realized under wave and wind excitations. Self-powered systems are fabricated based on the WS-TENG network, showing the capability of the device in real wave environment. The work provides a new driving paradigm that can further enhance the energy harvesting capability toward large-scale blue energy utilization based on TENGs.

1. Introduction

The use of fossil fuels leads to growing environmental threats to human society, which renders the urgency to reduce carbon emission and achieve carbon neutrality.[1] The development of renewable energy sources can alleviate the dependence on fossil or other non-renewable energy sources.[2] As one of the most promising clean and renewable energy sources, large-scale and efficient utilization of ocean blue energy remains a challenging problem to be solved. The wave energy is a typical ocean energy source that has been highly concerned and wildly investigated, for its large reserves, wide distribution and easy accessibility. Traditional technologies for wave energy collection based on electromagnetic generators (EMGs) still suffer from high cost, bulky and complex structure.[2b,3] The EMG usually achieve a high efficiency under high driving frequencies, while water waves have characteristics of low frequency, making complex transmission mechanisms necessary for the EMG-based devices.[4] On the contrary, the triboelectric nanogenerator (TENG) provides a new choice for wave energy acquisition, with low cost, light weight and relatively high response for low-frequency excitations.[5]

First invented in 2012, the TENG has been successfully developed to convert various mechanical energy into electrical energy, based on triboelectrification and electrostatic induction.[5b,f,6] By virtues of simple structure, easy fabrication, light weight, and rich material choices, the TENG and its networks exhibit advantageous results for wave energy harvesting.[7] However, up to now, most of the prototype designs are purely based on inertial eccentric structures with smooth outer shell to respond to water wave agitations. Because of the low-frequency characteristics of water waves, the inertial effect is usually small, which leads to limited interactions between the device and the wave with low power take-off (PTO) efficiency.[8] More effective wave capture measures are required to fully utilize the wave energy. In addition, coupled effects between TENGs in a network structure can further enhance the performance besides the strengthening of each single TENG units, enabling large-scale wave energy harvesting.[5a,c,d,7k]

Here, a novel wheel-structured triboelectric nanogenerator (WS-TENG) with hyperelastic networking is designed for gentle

Y. Hu
School of Resources
Environment and Materials
Guangxi University
Nanning 530004, P. R. China

Y. Hu, H. Qiu, Q. Sun, Z. L. Wang, L. Xu
Beijing Institute of Nanoenergy and Nanosystems
Chinese Academy of Sciences
Beijing 101400, P. R. China
E-mail: zlwang@gatech.edu; xuliang@binn.cas.cn

Y. Hu, H. Qiu, Q. Sun, Z. L. Wang, L. Xu
Center on Nanoenergy Research
School of Physical Science and Technology
Guangxi University
Nanning 530004, P. R. China

Q. Sun, L. Xu
School of Nanoscience and Technology
University of Chinese Academy of Sciences
Beijing 100049, P. R. China

Z. L. Wang
Georgia Institute of Technology
Atlanta, Georgia 30332-0245, USA

**ADVANCED
SCIENCE NEWS**

www.advancedsciencenews.com
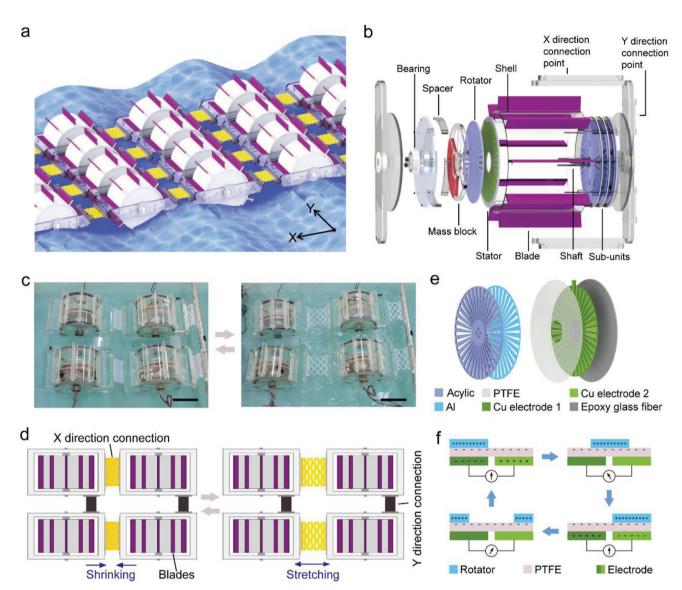
**small
methods**

www.small-methods.com

Figure 1. Structure and working principle of the TENG. a) Schematic illustration of the TENG network for large-scale wave energy harvesting. b) Schematic explosive view of the device. c) Photographs of the TENG network working in water. Scale bar, 10 cm. d) Schematic illustrations of the TENG network working in water. e) Structure of the rotator and stator. f) Schematics of working principle of the TENG sub-unit.

wave energy harvesting. The external blades on the shell of the TENG enhance the interaction between the wave and the device, enabling rolling on the water surface like a wheel, which can continuously agitate the TENG. Meanwhile, the hyperelastic network structure connects WS-TENGs to form a network that can stretch and contract like a spring, further enhances the motion of the device. Under the agitation of waves or even wind, a variety of driving modes with synergistic effects can be achieved. The performance of the device is characterized in detail, and the network is validated in wave tank experiments. Moreover, self-powered systems based on the WS-TENG network are also successfully demonstrated. The work provides a new general driving paradigm applicable to various TENG configurations, which can further enhance the energy harvesting capability toward large-scale blue energy utilization.

2. Results and Discussion

2.1. Device Structure and Working Principle

As shown in **Figure 1**a, the WS-TENGs with external blades are networked via the connection structure. Under the excitation of water waves, the hyperelastic connection along X direction can repeatedly stretch and shrink, contributing to arousing the device shell to roll on water surface. An explosive view of the WS-TENG unit is demonstrated in Figure 1b. The device is mainly constituted by a packaging shell with blades, a frame for connection, and TENG sub-units which are formed by rotator disks, stator disks, and swinging eccentric structures with mass blocks. Blades are evenly adhered on the surface of the shell for enhancing the interaction with water waves, forming a shape similar to wheels.

**ADVANCED
SCIENCE NEWS**

www.advancedsciencenews.com
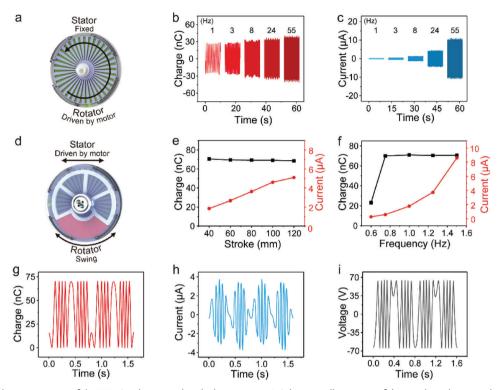
**small
methods**

www.small-methods.com

Figure 2. Electrical measurement of the TENG sub-unit under ideal agitations. a) Schematic illustration of driving the sub-unit with direct rotation. b,c) Transferred charges (b) and short-circuit current (c) of the sub-unit with different rotation speeds. The speed is noted by the output signal frequency. d) Schematic illustration of reciprocally driving the sub-unit with the rotator swinging freely. e) Transferred charges and short-circuit current of the sub-unit under different driving stokes. f) Transferred charges and short-circuit current of the sub-unit under different driving frequencies. g–i) Detailed output profiles of transferred charges (g), short-circuit current (h), and open-circuit voltage (i) of the sub-unit in two driving cycles. (g-i) are measured under a driving stoke of 80 mm and a frequency of 1.25 Hz.

The shell is fixed with stator disks, while the eccentric structures are fixed with rotator disks. The rectangular frame is used to mount the shell, which can be connected by X and Y connection structures through the connection points to form a large network. Details of the connection structures are shown in Figures S1 and S2 (Supporting Information). The connection structure along the X direction is a silicone plate with meshes (Figure S3, Supporting Information). The structure has nonlinearity in stress-strain behavior and can have large elastic stretching, showing hyperelasticity adaptive to wave energy harvesting.

Figure 1c demonstrates the photograph of the WS-TENG network working in water, and the X connection structures are shown to stretch and shrink under water waves, inducing the shell to roll along with direct wave agitations (Movie S1, Supporting Information). In the process, the X connection can couple different TENG units in the network with storing and releasing wave energy, enhancing the capability of wave energy harvesting. The Y connection structure can keep the Y distance of devices and absorb the impact energy to relieve damage. The corresponding network structure is more clearly demonstrated in Figure 1d.

Details of the rotator and stator disks are shown in Figure 1e, which adopt a radial grating structure with a periodicity of 10°. For the rotator disk, a grating-structured Al film is adhered on an acrylic substrate as a triboelectric material. For the stator disk, a polytetrafluoroethylene (PTFE) film is adhered on a Cu layer con-sisting of two Cu electrodes, which are fabricated on an epoxy glass fiber substrate through the printed circuit board (PCB) technics. The working mechanism of the sub-unit is shown in Figure 1f, which is a conjugation of triboelectrification and electrostatic induction. With the relative rotation of the rotator and the stator, the PTFE and Al layers are triboelectrified. Then free electrons are induced to transfer between the two Cu electrodes following the motion of the charged Al layer, generating alternating current in the external circuit.[9] For the WS-TENG in water waves, the relative motion of the rotator and the stator can be triggered by the roll of the shell or the impact-induced swing of the mass block, which will be discussed in detail later.

2.2. Electrical Characterization of the WS-TENG in Air

To test the fundamental output characteristics of the WS-TENG under ideal agitations, two driving modes by motors are applied. As shown in **Figure 2**a, in the first mode, the stator is fixed, and the rotator is driven directly by a rotary motor. The output capability of a single sub-unit was tested at different rotation speeds. As the speed increases, the frequency of the output signal rises synchronously, and the transferred charges are enhanced slowly to ≈77.6 nC with a signal frequency of 55 Hz (Figure 2b). Meanwhile, the peak value of short-circuit current increases fast and reaches 11.01 µA (Figure 2c). The trend of the

ADVANCED
SCIENCE NEWS
www.advancedsciencenews.com
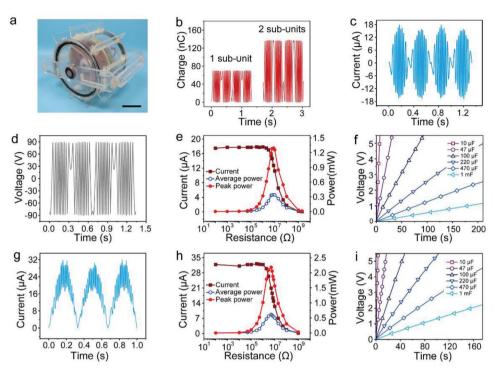
small
methods
www.small-methods.com

Figure 3. Electrical measurement of the WS-TENG under ideal agitations. a) Photograph of the fabricated WS-TENG. Scale bar, 6.5 cm. b) Transferred charges of different amounts of sub-units in the WS-TENG. c-d) Short-circuit current (c) and open-circuit voltage (d) of the WS-TENG with 2 sub-units. e) Peak current, peak power and average power of the WS-TENG under various resistive loads. f) Voltage of different capacitors charged by the WS-TENG. g) Rectified current of two WS-TENGs. h) Peak current, peak power and average power of two WS-TENGs under various resistive loads. i) Voltage of different capacitors charged by two WS-TENGs. The data are measured with a driving stroke of 80 mm and a frequency of 1.5 Hz.

open-circuit voltage is generally consistent with the amount of charges, with a peak-to-peak value of ≈151.6 V for 55 Hz (Figure S4, Supporting Information).

In order to simulate the motion of the WS-TENG by impacts of water waves, another mode is to excite the stator by a linear motor in a reciprocal way, and the rotator and mass block will swing freely, as shown in Figure 2d. The dependence of the output performance of a sub-unit on the agitation amplitude and frequency is explored. As shown in Figure 2e, at a frequency of 1.25 Hz, the amount of transferred charges remains stable, while the current increases almost linearly with increasing stroke, reaching up to 5.10 µA at a stroke of 120 mm. The corresponding peak-to-peak voltage remains steady at ≈126 V (Figure S5, Supporting Information). Under a stroke of 80 mm, with the increase of driving frequency, the peak value of current also increases, and the value of transferred charges remains almost unchanged, except for the one at the frequency of 0.5 Hz, where the excited relative angular displacement of the rotator and stator may be lower than one period of the radial grating (Figure 2f). The short-circuit current is related to the velocity of the relative motion according to $I = dQ/dt$, so it will alter obviously with varying stroke or frequency. In addition, the trend of open-circuit voltage is consistent with charge, as illustrated in Figure S6 (Supporting Information). Such characteristic originates from the periodic radial grating structure of the device. The peak values of charge and voltage can be achieved in the process when the relative motion of the rotator and stator reaches one period of the radial grating.[10] Moreover, detailed output profiles of the sub-unit in two driving cycles

under a typical excitation condition are shown in Figures 2g–i. The transferred charges remain steady at ≈67.13 nC under an excitation frequency of 1.25 Hz and a stroke of 80 mm. The short-circuit current and peak-to-peak open-circuit voltage of the sub-unit can reach ≈3.8 µA and 126 V, respectively. In addition, the transferred charges of a sub-unit under long-term operation were also tested, and the output is very stable after the initial stage (Figure S7, Supporting Information).

Figure 3a shows a fabricated WS-TENG unit with 2 sub-units, which was tested by the linear motor simulating wave agitations in water. The charge output of the WS-TENG with 2 sub-units reaches ≈137.5 nC under a frequency of 1.5 Hz and a stroke of 80 mm, which is almost twice as large as that of a single sub-unit (Figure 3b). The corresponding curves of the short-circuit current and open-circuit voltage are shown in Figure S8 (Supporting Information). Thus, the charge output of the WS-TENG can be almost linearly enhanced by integrating more TENG sub-units. Schematic diagram of the testing circuit is presented in Figure S9 (Supporting Information). Under the same agitation conditions, the short-circuit current and peak-to-peak open-circuit voltage of the WS-TENG are 17.86 µA and 180.21 V, respectively (Figures 3c,d). The output of the device under various resistive loads was also tested to characterize the output power. As shown in Figure 3e, the peak value of output current decreases with rising load resistance, and the maximum peak power and average power can reach 1.29 and 0.34 mW respectively, under an 8 MΩ load when agitated by a frequency of 1.5 Hz and a stroke of 80 mm. The average power is calculated

**ADVANCED
SCIENCE NEWS**

www.advancedsciencenews.com
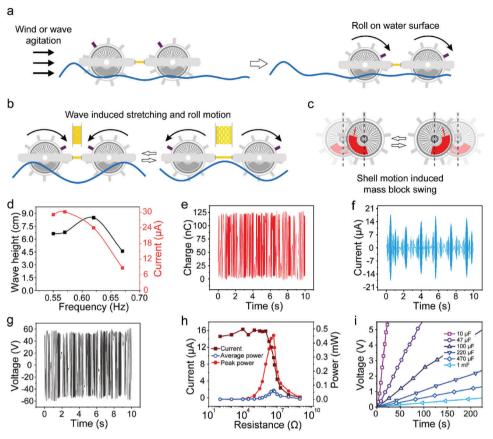
**small
methods**

www.small-methods.com

Figure 4. Working principle and characterization of the WS-TENG in water waves. a) Directional roll motion of the WS-TENG driven by waves or wind. b) Roll motion of the WS-TENG induced by stretching the networking structure in water waves. c) Swing motion of the inner mass block when the WS-TENG is impacted by waves. d) Output current and wave height under different wave frequencies. e-g) Transferred charges (e), short-circuit current (f), and open-circuit voltage (g) of a single WS-TENG in water waves. h) Peak current, peak power and average power of a single WS-TENG under various resistive loads. i) Voltage of different capacitors charged by a single WS-TENG in water. (e–i) are measured in water waves of 0.57 Hz.

by the following equation:

$$P_{ave} = \frac{\int_0^T I^2 R \, dt}{T} \tag{1}$$

where I is the output current, T is the period, and R is the load resistance. The corresponding average power density is 1.578 W m^{-3} considering the volume of the TENG sub-units with the mass blocks. It should be emphasized that the shell adopted here actually can accommodate more sub-units, with almost linearly augmented output charges. Under the same condition, the charging performance of the WS-TENG to different capacitors was measured. Capacitors of 10, 47, and 100 µF can be charged to 5.5 V in 6.76, 30.64, and 91.96 s, respectively, while capacitors of 220 µF, 470 µF, and 1 mF are charged to 3.92, 1.99, and 0.89 V in 160 s, respectively (Figure 3f).

To realize large-scale ocean wave energy harvesting, multiple WS-TENG units need to be connected into a network. The outputs of WS-TENG units should be rectified before merging together for the total output due to possible phase mismatch, as shown in Figure S10 (Supporting Information). Under an excitation frequency of 1.5 Hz and a stroke of 80 mm, the total rectified current of two WS-TENGs can attain 31.93 µA, demonstrating ev-

ident enhancement with device number, as shown in Figure 3g. The peak power and average power can be enhanced to 2.18 and 0.62 mW respectively, under a resistive load of 5 MΩ (Figure 3h), which are almost twice the outputs of a single device. As presented in Figure 3i, the charging rate is also significantly improved. It takes 3.67 s for a 10 µF capacitor to be charged to 5.5 V and a 1 mF capacitor can be charged to 2.05 V in 160 s.

2.3. Performance of the WS-TENG Network in Water

In water waves, the WS-TENG network can be agitated in three different modes, which can synergistically enhance the output of the device, as shown in **Figures** 4a–c. First, different from traditional designs of smooth shell, the external blades on the TENG allow tighter interaction between the wave and the device. Thus, when the network is imposed an imbalanced force from one side by wave or even by wind, the interconnected rectangular frames will move translationally, inducing the shells (stators) of the WS-TENGs to roll on the water surface like a wheel (Figure 4a). In this situation, the rotators will almost maintain their orientations due to the gravity of the mass blocks, resulting in relative motion between rotators and stators and producing output current
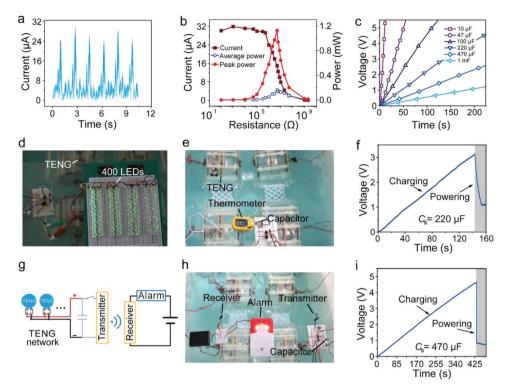
**ADVANCED
SCIENCE NEWS**

www.advancedsciencenews.com

**small
methods**

www.small-methods.com

Figure 5. Characterization and application of the WS-TENG network in water. a) Rectified short-circuit current of two networked WS-TENGs in water. b) Peak current, peak power, and average power of two networked WS-TENGs under various resistive loads. c) Voltage of different capacitors charged by two networked WS-TENGs in water. d) 400 LEDs lighted up directly by the WS-TENG network. e) Photograph of the WS-TENG network powering a thermometer. f) Charging and discharging profile for the thermometer powered by the TENG network. g) Schematic diagram of a wireless signal transmitting system powered by the TENG network. h) Photograph of the wireless transmitting powered by the TENG network. i) Charging and discharging profile for powering the transmitter by the TENG network. The data are measured in water waves of 0.57 Hz.

continuously. Second, under the excitation of water waves, the hyperelastic connection along X direction can repeatedly stretch and shrink with wave energy storing and releasing, inducing relative motion among connected rectangular frames, which will also arouse the shells to roll on water surface (Figure 4b). Third, when the WS-TENGs are impacted by waves, the eccentric structures with mass blocks will swing like a pendulum (Figure 4c), inducing relative motion between the rotators and stators, similar to the traditional agitation mode.[10] The multiple driving modes can have synergistic effects under wave and wind excitations, enhancing the energy harvesting capability of the device.

To characterize the performance in a real water environment, a WS-TENG network consisting of four WS-TENG units was tested in a wave tank. The network was first agitated with waves of different frequencies, and the corresponding wave height was also recorded, which is averaged over five different positions (Figure S11, Supporting Information). Taking the outputs of two units in the network as a reference, the rectified current can reach a maximum with a frequency of 0.57 Hz (Figure 4d). The wave height is affected by the dimension of the wave tank, which can achieve a maximum value at certain frequency. The device in water seems to have some resonance effect and is more sensitive to frequency rather than wave height. Based on the above optimized test condition, the electrical output of the WS-TENG network is further characterized in water. Figures 4e–g demonstrate the basic electrical outputs of a single WS-TENG with two sub-units in

the network. The amount of transferred charges is ≈122.23 nC. The short-circuit current can reach 17.04 µA and the peak-to-peak open-circuit voltage can achieve over 116 V.

The power outputs of the WS-TENG with different resistive loads were also tested. The peak power and average power can reach 0.45 and 0.0627 mW respectively, under a load of 5 MΩ (Figure 4h). Still, the power can be further enhanced by integrating more sub-units to fully use the inner space of the device. Figure 4i demonstrates the charging capability of the device in water, capacitors of 10 and 47 µF are charged to 5.5 V in 20.7 and 99.7 s respectively, and capacitors of 100 µF, 220 µF, 470 µF and 1 mF are charged to 4.42, 2.05, 1.16, and 0.5 V, respectively, in 200 s.

Figure 5a shows the rectified current of two units in the network, which reaches ≈29.89 µA, nearly doubling that of a single device under wave excitations. The peak power and average power can achieve 1.125 and 0.1612 mW respectively, under a load resistance of 5 MΩ (Figure 5b). Their charging performance to capacitors agitated by waves was also characterized, as shown in Figure 5c. A 10 µF capacitor can be charged to 5.5 V in 13.49 s, while the voltage of a 1 mF capacitor reaches 1.06 V within 200 s.

To visually confirm the excellent performance of the WS-TENG network, 400 commercial light-emitting diodes (LEDs) were used as a load for two units in the network. As shown in Figure 5d; Movie S2 (Supporting Information) the LEDs can be lighted up simultaneously. A self-powered system can also be

**ADVANCED
SCIENCE NEWS**

www.advancedsciencenews.com

**small
methods**

www.small-methods.com

constructed based on the harvested wave energy. In the system, a storage capacitor can be used to store the energy collected by the network in advance and supply power to electronics when the voltage meets the requirement. As a demonstration, Figure 5e shows a self-powered temperature sensing system using the WS-TENG network. A storage capacitor of 220 μF is charged to 3.13 V within 143.5 s by the network, which is then used to power the thermometer to obtain temperature data without a battery (Figures 5e,f; Movie S3, Supporting Information). Schematic diagram of the circuit is presented in Figure S12 (Supporting Information). The data can be further transmitted by a self-powered wireless system, as shown in Figure 5g. A capacitor of 470 μF is charged to 4.65 V in 432.31 s by the network, which successfully powers the transmitter to send wireless signals, and the alarm lights on at the receiver side to indicate the signal transmitting (Figures 5h,i; Movie S4, Supporting Information). The demonstrations confirm the WS-TENG network as a promising candidate for blue energy harvesting and constructing self-powered marine systems, which should be meaningful for future ocean research and development.

3. Conclusion

In this work, a wheel-structured triboelectric nanogenerator with hyperelastic networking is designed for effective wave energy harvesting. By contrast to the traditional designs of a smooth shell, the external blades on the TENG allow tighter interaction between the wave and the device, which can roll on the water surface like a wheel, continuously agitating relative rotation of radial grating rotators and stators of the TENG sub-units. The hyperelastic networking structure can enhance the motion of the shell by storing and releasing wave energy like a spring and connect the WS-TENGs to form a large-scale network. Meanwhile, the internal eccentric structure fixed with the rotator can swing like a pendulum under impact. Such multiple driving modes with synergistic effects can be realized under wave and wind excitations, enhancing the power take-off compared with traditional designs. The excellent performance of the device is characterized in detail, and the network is validated in wave tank experiments. Self-powered systems for sensing and wireless signal transmitting based on the WS-TENG network are also demonstrated. The work provides a new general driving paradigm applicable to various TENG configurations, which can further enhance the energy harvesting capability toward large-scale blue energy utilization.

4. Experimental Section

Fabrication of the TENG Unit: The substrate of the stator was an epoxy glass fiber sheet (2 mm thickness) with an inner diameter of 32 mm and an outer diameter of 140 mm. The electrode layer of copper (35 μm thickness) with complementary sectors that had the same central angle of ≈5° was fabricated on the substrate through the PCB techniques, and a PTFE film with a thickness of 50 μm was adhered on the surface. For the rotator, an aluminum film (50 μm thickness) was adhered on the acrylic substrate with a diameter of 127 mm and cut to the same shape as the substrate. The spacing between stators was controlled by spacers near the outer edge, and the spacing between rotators was controlled by central circular spacers passing through the shaft. Sector-shaped copper blocks with a 120° central angle (62 mm inner diameter and 124 mm outer diameter) were used as mass blocks. The stators were connected by screws at the edge, and the rotators were connected coaxially by shafts from the center, with mass blocks. The shaft was then mounted in a water-proof acrylic cylindrical shell via bearings. The blades with a length of 130 mm and a width of 24 mm (4 mm thickness) were evenly attached to the shell. The whole shell was then mounted on the frame (250 mm length and 52 mm width) via bearings.

Fabrication of the Network: The connection structure of X direction was prepared using a silicone plate with a Shore hardness of 30 (90 mm length and 48 mm width), in which meshes were fabricated by cutting. The connection structure of Y direction was prepared using a silicone plate with a Shore hardness of 65 (50 mm length and 40 mm width). Both ends of the silicone plate were adhered to a piece of acrylic plate, which was then inserted into the corresponding U-shaped groove on the frame to connect TENG units into a network (Figures S1 and S2, Supporting Information).

Electrical Measurement of the Device: The transferred charges, current, and voltage were measured by an electrometer (Keithley 6514). The data were collected mainly by a data acquisition card (NI USB–6356) and a LabVIEW program. The device was driven by a rotary motor and a linear motor (LinMot) during testing basic performance in air. Eight wave makers (RW-20) were used to produce water waves in a wave tank with a dimension of 1.32 m × 0.81 m.

Supporting Information

Supporting Information is available from the Wiley Online Library or from the author.

Conflict of Interest

The authors declare no conflict of interest.

Author Contributions

Y.H. and H.Q. contributed equally to this work. L.X. conceived the idea. L.X., Y.H., and H.Q. designed the device and experiments. Y.H. and H.Q. fabricated the device and did the experiments. Y.H., L.X., and H.Q. discussed the data and prepared the figures. L.X., Y.H., H.Q., Q.S., and Z.L.W. wrote and revised the manuscript. L.X. and Z.L.W. guided the project.

Data Availability Statement

The data that support the findings of this study are available from the corresponding author upon reasonable request.

**ADVANCED
SCIENCE NEWS**

www.advancedsciencenews.com

**small
methods**

www.small-methods.com

[1] A. Timmermann, J. Oberhuber, A. Bacher, M. Esch, M. Latif, E. Roeckner, *Nature* **1999**, *398*, 694.

[2] a) D. Gielen, F. Boshell, D. Saygin, *Nat. Mater.* **2016**, *15*, 117; b) J. Tollefson, *Nature* **2014**, *508*, 302; c) P. V. Kamat, *J. Phys. Chem. C* **2007**, *111*, 2834.

[3] a) A. F. D. Falcao, *Renewable Sustainable Energy Rev.* **2010**, *14*, 899; b) E. Callaway, *Nature* **2007**, *450*, 156; c) O. Ellabban, H. Abu-Rub, F. Blaabjerg, *Renewable Sustainable Energy Rev.* **2014**, *39*, 748.

[4] a) J. Falnes, *Mar. Struct.* **2007**, *20*, 185; b) R. Henderson, *Renewable Energy* **2006**, *31*, 271; c) B. Drew, A. R. Plummer, M. N. Sahinkaya, *Proc. Inst. Mech. Eng., Part A* **2009**, *223*, 887.

[5] a) Z. L. Wang, *Nature* **2017**, *542*, 159; b) C. S. Wu, A. C. Wang, W. B. Ding, H. Y. Guo, Z. L. Wang, *Adv. Energy Mater.* **2019**, *9*, 1802906; c) X. D. Yang, L. Xu, P. Lin, W. Zhong, Y. Bai, J. J. Luo, J. Chen, Z. L. Wang, *Nano Energy* **2019**, *60*, 404; d) L. Xu, T. Jiang, P. Lin, J. J. Shao, C. He, W. Zhong, X. Y. Chen, Z. L. Wang, *ACS Nano* **2018**, *12*, 1849; e) H. M. Wang, L. Xu, Z. L. Wang, *Nanoenergy Advances* **2021**, *1*, 32; f) Z. L. Wang, *Faraday Discuss.* **2014**, *176*, 447; g) N. N. Zhai, Z. Wen, X. P. Chen, A. M. Wei, M. Sha, J. J. Fu, Y. N. Liu, J. Zhong, X. H. Sun, *Adv. Energy Mater.* **2020**, *10*, 2001041; h) X. L. Wei, Z. Wen, Y. N. Liu, N. N. Zhai, A. M. Wei, K. Feng, G. T. Yuan, J. Zhong, Y. H. Qiang, X. H. Sun, *Nano-Micro Lett.* **2020**, *12*, 1.

[6] a) F. R. Fan, Z. Q. Tian, Z. L. Wang, *Nano Energy* **2012**, *1*, 328; b) Z. L. Wang, *Mater. Today.* **2017**, *20*, 74; c) Z. L. Wang, J. Chen, L. Lin, *Energy Environ. Sci.* **2015**, *8*, 2250; d) S. Niu, Z. L. Wang, *Nano Energy* **2015**, *14*, 161.

[7] a) J. Wang, S. Li, F. Yi, Y. Zi, J. Lin, X. Wang, Y. Xu, Z. L. Wang, *Nat. Commun.* **2016**, *7*, 12744; b) J. Bae, J. Lee, S. Kim, J. Ha, B. S. Lee, Y. Park, C. Choong, J. B. Kim, Z. L. Wang, H. Y. Kim, J. J. Park, U. I. Chung, *Nat. Commun.* **2014**, *5*, 4929; c) Z. L. Wang, T. Jiang, L. Xu, *Nano Energy* **2017**, *39*, 9; d) L. Xu, Y. K. Pang, C. Zhang, T. Jiang, X. Y. Chen, J. J. Luo, W. Tang, X. Cao, Z. L. Wang, *Nano Energy* **2017**, *31*, 351; e) H. F. Qin, L. Xu, S. Q. Lin, F. Zhan, K. Dong, K. Han, H. M. Wang, Y. W. Feng, Z. L. Wang, *Adv. Funct. Mater.* **2022**, *32*, 2111662; f) L. Q. Liu, X. Y. Yang, L. L. Zhao, H. X. Hong, H. Cui, J. L. Duan, Q. M. Yang, Q. W. Tang, *ACS Nano* **2021**, *15*, 9412; g) H. M. Wang, L. Xu, Y. Bai, Z. L. Wang, *Nat. Commun.* **2020**, *11*, 4203; h) C. G. Zhang, L. X. He, L. L. Zhou, O. Yang, W. Yuan, X. L. Wei, Y. B. Liu, L. Lu, J. Wang, Z. L. Wang, *Joule* **2021**, *5*, 1613; i) X. K. Xie, X. P. Chen, C. Zhao, Y. N. Liu, X. H. Sun, C. Z. Zhao, Z. Wen, *Nano Energy* **2021**, *79*, 105439; j) L. J. Xie, N. N. Zhai, Y. N. Liu, Z. Wen, X. H. Sun, *Research* **2021**, *2021*, 9143762; k) H. J. Qiu, H. M. Wang, L. Xu, M. L. Zheng, Z. L. Wang, *Energy Environ. Sci.* **2023**, *16*, 473.

[8] a) X. F. Wang, S. M. Niu, Y. J. Yin, F. Yi, Z. You, Z. L. Wang, *Adv. Energy Mater.* **2015**, *5*, 1501467; b) W. B. Liu, L. Xu, T. Z. Bu, H. Yang, G. X. Liu, W. J. Li, Y. K. Pang, C. X. Hu, C. Zhang, T. H. Cheng, *Nano Energy* **2019**, *58*, 499; c) J. Chen, J. Yang, Z. L. Li, X. Fan, Y. L. Zi, Q. S. Jing, H. Y. Guo, Z. Wen, K. C. Pradel, S. M. Niu, Z. L. Wang, *ACS Nano* **2015**, *9*, 3324.

[9] S. M. Niu, Y. Liu, X. Chen, S. Wang, Y. S. Zhou, L. Lin, Y. Xie, Z. L. Wang, *Nano Energy* **2015**, *12*, 760.

[10] Y. Bai, L. Xu, C. He, L. P. Zhu, X. D. Yang, T. Jiang, J. H. Nie, W. Zhong, Z. L. Wang, *Nano Energy* **2019**, *66*, 104117.